MOLECULAR GAS IN 3C 293: THE FIRST DETECTION OF CO EMISSION AND ABSORPTION IN AN FANAROFF-RILEY TYPE II RADIO GALAXY

A. S. EVANS

Division of Physics, Math, and Astronomy MS 105-24, California Institute of Technology, Pasadena, CA 91125; ase@astro.caltech.edu

D. B. SANDERS AND J. A. SURACE[1]

Institute for Astronomy, 2680 Woodlawn Drive, Honolulu, HI 96822; sanders@ifa.hawaii.edu, jason@ipac.caltech.edu

AND

J. M. MAZZARELLA

IPAC, MS 100-22, California Institute of Technology, Jet Propulsion Laboratory, Pasadena, CA 91125; mazz@ipac.caltech.edu

ABSTRACT

The first detection of CO emission in a Fanaroff and Riley type II (i.e., edge-brightened radio lobe morphology) radio galaxy is presented. Multiwavelength (0.36–2.17 μm) imaging of 3C 293 shows it to be a disk galaxy with an optical jet or tidal tail extending toward what appears to be a companion galaxy 28 kpc away via a low surface brightness envelope. The molecular gas appears to be distributed in an asymmetric disk rotating around an unresolved continuum source, which is presumably emission from the active galactic nucleus (AGN). A narrow ($\Delta v_{abs} \sim 60$ km s^{-1}) absorption feature is also observed in the CO spectrum and is coincident with the continuum source. Assuming the standard CO conversion factor, the molecular gas (H$_2$) mass is calculated to be 1.5×10^{10} $M_\odot$, several times the molecular gas mass of the Milky Way. The high concentration of molecular gas within the central 3 kpc of 3C 293, combined with the multiwavelength morphological peculiarities, supports the idea that the radio activity has been triggered by a gas-rich galaxy-galaxy interaction or merger event.

Subject headings: galaxies: active — galaxies: individual (3C 293) — galaxies: ISM — infrared: galaxies — ISM: molecules — radio lines: galaxies

1. INTRODUCTION

Substantial evidence exists that galaxy interactions or mergers are the trigger for the nuclear activity in radio galaxies. Optical imaging surveys by Heckman et al. (1986) and Smith & Heckman (1989a, 1989b) have shown that a significant fraction of low-redshift powerful ($P_{408 \text{ MHz}} \gtrsim 3 \times 10^{25}$ W Hz^{-1}) radio galaxies possess morphological peculiarities (e.g., tails, fans, bridges, and dust lanes) commonly associated with the collisions of galaxies. A significant fraction of low-redshift radio galaxies is also known to be luminous far-infrared sources (Golombek, Miley, & Neugebauer 1988). In many cases, the shape of the spectral energy distributions (SEDs) at mid- and far-infrared wavelengths is consistent with thermal emission from dust heated by young massive stars and/or the active galactic nucleus (AGN).

Improvements in millimeter receiver technology and the availability of moderate size (i.e., total collecting area greater than 500 square meters) millimeter arrays has made it possible to detect and spatially map star-forming molecular gas in radio galaxies. Molecular gas, which forms on the surface of dust grains, is of particular interest in active galaxies because it is also a likely source of fuel for the central engine during the initial phases of the merger. To date, several low-redshift radio galaxies have been unambiguously detected with single-dish telescopes, revealing substantial quantities (1×10^9 to 5×10^{10} $M_\odot$) of molecular gas (Phillips et al. 1987; Mirabel, Sanders, & Kazès 1989; Mazzarella et al. 1993; Evans 1998; Evans et al. 1999a). To date, however, detections of CO emission have been limited to radio compact and Fanaroff and Riley I (edge-darkened radio lobe morphology; Fanaroff & Riley 1974) radio galaxies, the latter of which tend to have relatively weak radio power.

In this paper, the first detection of CO emission and absorption in a Fanaroff and Riley II (edge-brightened radio lobe morphology) radio galaxy, 3C 293 ($P_{408 \text{ MHz}} \sim 4.5 \times 10^{25}$ W Hz^{-1}), is presented. The galaxy possesses optical morphological peculiarities and extended radio and CO emission, which makes it an ideal source for studying the relationship between emission in radio galaxies at multiple wavelengths.

The paper is divided into five sections. Section 2 is a discussion of the optical, near-infrared, and millimeter observations of 3C 293. The data reduction methods and molecular gas mass calculations are summarized in § 3. Section 4 contains an estimate of the dynamical mass of 3C 293 based on the CO data, a discussion of the 2.7 mm continuum emission and CO absorption, and a detailed comparison of the morphologies of the galaxy at optical, near-infrared, millimeter, and radio wavelengths. Section 5 summarizes the results.

Throughout this paper, we adopt $H_0 = 75$ km s^{-1} Mpc^{-1} and $q_0 = 0.0$. Thus, for a source at a redshift of 0.045, 815 pc subtends 1$''$ in the sky plane.

2. OBSERVATIONS

The interpretation of the CO data presented in this paper has benefited from observations of the galaxy at other wavelengths. Below, the ground-based U'-, B-, I-, and K'-band imaging observations, as well as the millimeter

---

observations, are summarized.[2] Additional radio data and *Hubble Space Telescope* (*HST*) data have also been obtained courtesy of J. P. Leahy and the *HST* Archive.

2.1. *Ground-based Imaging*

Ground-based imaging observations of 3C 293 were made at the University of Hawaii (UH) 2.2 m telescope. The U'-, B-, and I-band images were obtained on 1998 March 25 using the Orbit Semiconductor 2048×2048 CCD camera. The original scale is $0\rlap{.}''09$ pixel^{-1} (Wainscoat 1996), but the CCD was read out with 2×2 pixel binning. Four dithered exposures were taken, with integration times of 480, 360, and 360 s each for U', B, and I, respectively. Near-infrared, K' observations of 3C 293 were also obtained on 1996 April 24 using the UH Quick Infrared Camera (QUIRC; Hodapp et al. 1996), which consists of a 1024×1024 pixel HgCdTe Astronomical Wide Area Infrared Imaging (HAWAII) array. The near-infrared observations were done at f/10, providing a field of view of $3' \times 3'$. Five dithered exposures were taken, each with an integration time of 180 s.

2.2. CO *Spectroscopy*

The initial millimeter observations of 3C 293 were made with the NRAO[3] 12 m telescope on 1996 January 24. The telescope was configured with two 256×2 MHz channel filterbanks and dual polarization SIS spectral line receivers tuned to the frequency 110.35 GHz, corresponding to a redshift of 0.045 (Sandage 1966; Burbidge 1967) for the $CO(1 \rightarrow 0)$ emission line. Observations were obtained using a nutating subreflector with a chop rate of ~ 1.25 Hz. Six minute scans were taken, and a calibration was done every other scan. Pointing was done on 3C 273 prior to the observations, and the pointing was checked at the end of the observations using Mars. The total duration of the observations was 8.8 hr.

Follow-up aperture synthesis maps of $CO(1 \rightarrow 0)$ and 2.7 mm continuum emission in 3C 293 were made with the Owens Valley Radio Observatory (OVRO) Millimeter Array during three observing periods from 1997 September to November. The array consists of six 10.4 m telescopes, and the longest observed baseline was 242 m. Each telescope was configured with 120×4 MHz digital correlators. Observations done in the low-resolution configuration (1997 September and October) provided a $\sim 4\rlap{.}''0$ (FWHM) synthesized beam with natural weighting, and observations in the high-resolution configuration (1997 November) provided a beam of $\sim 2\rlap{.}''5$ (FWHM). During the observations, the nearby quasar HB 89 1308+326 (1.27 Jy at 110 GHz; B1950.0 coordinates $13^h08^m07\rlap{.}^s56$, $+32°36'40\rlap{.}''23$) was observed every 25 minutes to monitor phase and gain variations, and 3C 273 was observed to determine the passband structure. Finally, observations of Uranus were made for absolute flux calibration.

3. DATA REDUCTION AND RESULTS

3.1. *Imaging Data*

The U'-, B-, and I-band data reduction was performed using IRAF. The data reduction consisted of flat-fielding individual images, scaling each image to its median value to correct for offsets in individual images, then shifting and

median combining the images. The final images were then boxcar smoothed by 4×4 pixels.

Figure 1 shows two three-color images of 3C 293. In Figure 1*a*, 3C 293 is presented in a linear stretch to show the highest surface brightness features. Figure 1*b* shows the galaxy with a logarithm stretch, which reveals additional, extended low surface brightness structure.

The K'-band data reduction was done in a similar manner to the U'-, B-, and I-band data reduction, except that after the median level of each image was subtracted, the individual frames were averaged together without spatial shifting using a min/max averaging routine. This procedure removes the contribution of astronomical sources in the individual frames to produce an object-free "sky" image. This sky image was then subtracted from the individual frames before they were shifted and averaged. The resultant wide-field K'-band image is discussed in § 4.5.

3.2. *NRAO* 12 m *Telescope Data*

The NRAO 12 m telescope data were reduced using the IRAM data reduction package CLASS. The individual scans were checked for baseline instabilities, then averaged together. The emission line was observed to span the velocity range -500 to 350 km s^{-1} (where 0 km s^{-1} corresponds to the systemic velocity of 3C 293); thus a linear baseline was subtracted excluding this velocity range. The spectrum was then smoothed to 43 km s^{-1}.

Figure 2 shows the $CO(1 \rightarrow 0)$ spectrum. The emission line is moderately broad—the velocity width at half the maximum intensity, Δv_{FWHM}, of ~ 400 km s^{-1}. For comparison, the mean value for infrared luminous galaxies is 250 km s^{-1} (Sanders, Scoville, & Soifer 1991). An absorption feature is also observed at the systemic velocity of 3C 293 ($\sim 13,500$ km s^{-1}), which corresponds to the velocity of the H I absorption feature associated with the galaxy (Baan & Haschick 1981).

The CO emission line has a intensity, $I_{\mathrm{CO}} = T_{\mathrm{mb}} \Delta v$, of 2.0 ± 0.4 K km s^{-1}, where T_{mb} is the main-beam brightness temperature. Assuming a Kelvin-to-Jansky conversion factor of 25.2 Jy K^{-1} (P. Jewell 1995, private communication), the emission-line flux, $S_{\mathrm{CO}} \Delta v$, is 51 ± 11 Jy km s^{-1}.

3.3. *OVRO Data*

The OVRO data were reduced and calibrated using the standard Owens Valley array program MMA (Scoville et al. 1992). The data were then exported to the mapping program DIFMAP (Shepherd, Pearson, & Taylor 1995).

The resultant continuum and integrated intensity maps are shown in Figure 3. The CO emission in 3C 293 is extended over a region $7''$ (5.7 kpc) in diameter. Four spectra have also been extracted, showing clearly the narrow absorption feature ($\Delta v_{\mathrm{abs}} \sim 60$ km s^{-1}) seen in the single-dish spectrum. In contrast to the CO emission, the continuum emission is unresolved and appears to be located at the center of the molecular gas morphology. Both the synthesized maps of the CO absorption (not shown) and the 2.7 mm continuum are spatially coincident, which indicates the presence of CO-emitting gas along the line of sight to the continuum source.

The total flux measured within a $7''$ diameter aperture is 53 ± 10 Jy km s^{-1}, consistent with the flux obtained from the 12 m in a $74''$ beam.
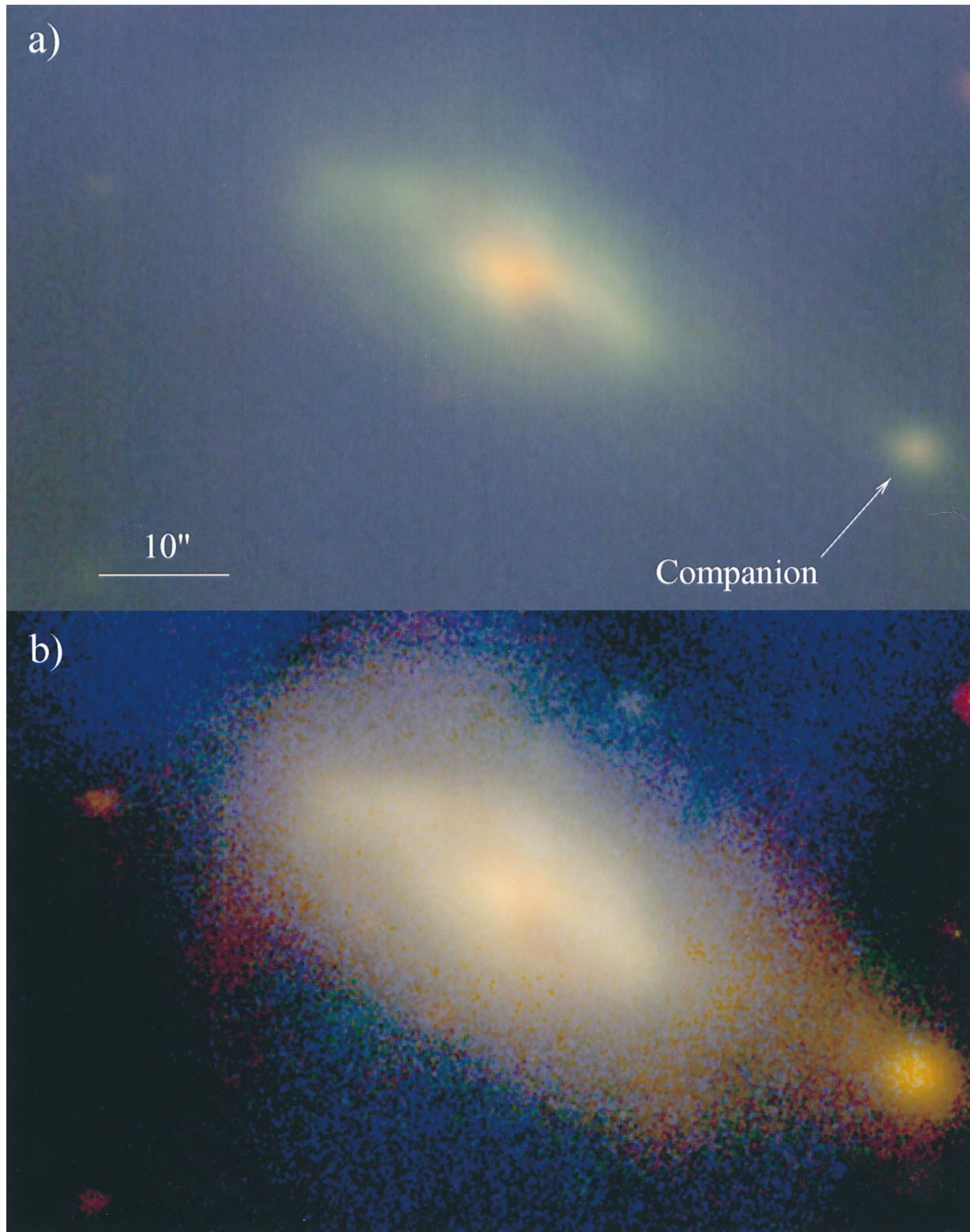
FIG. 1.—U'-, B-, and I-band images of 3C 293. The U-, B-, and I-band images are displayed as blue, green, and red, respectively. The images are shown with (a) linear and (b) logarithmic stretches. North is up, and east is to the left.

3.4. Molecular Gas Mass

For a $q_0 = 0.0$ universe, the luminosity distance for a source at a given redshift, z, is

$$D_L = cH_0^{-1}z(1 + 0.5z)(\text{Mpc}) . \qquad (1)$$

Given the measured flux, $S_{\text{CO}} \Delta v$, the CO luminosity of a source at redshift z is

$$L'_{\text{CO}} = \left(\frac{c^2}{2kv_{\text{obs}}^2}\right) S_{\text{CO}} \Delta v D_L^2 (1 + z)^{-3} , \qquad (2)$$

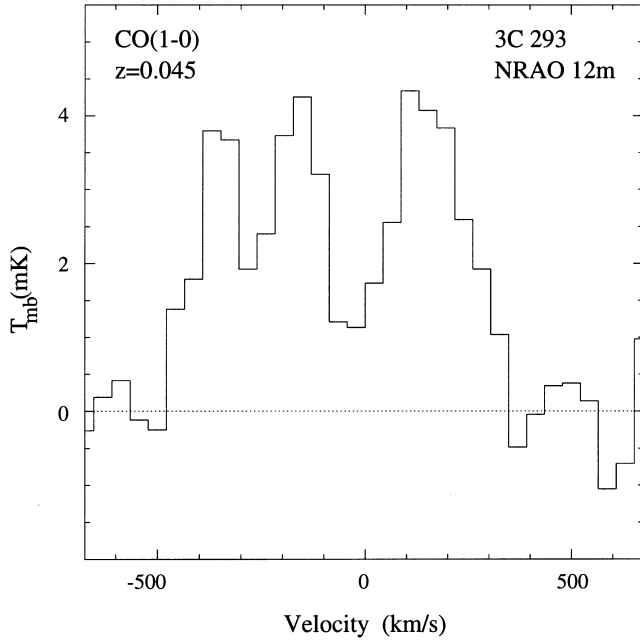FIG. 2.—NRAO 12 m CO(1 → 0) spectrum of 3C 293. The spectrum is plotted in units of main-beam brightness temperature. The spectrum has a 1 σ rms of 0.52 mK per velocity channel, where the resolution of a single channel is ~43 km s^{-1}.

where c is the speed of light, k is the Boltzmann constant, and ν_{obs} is the observed frequency. For a luminosity distance expressed in units of Mpc, L'_{CO} can be written as

$$L'_{CO} = 2.4 \times 10^3 \left(\frac{S_{CO}\,\Delta v}{\text{Jy km s}^{-1}}\right)\left(\frac{D_L^2}{\text{Mpc}^2}\right)(1 + z)^{-1}$$

$$(\text{K km s}^{-1}\text{ pc}^2) \ . \quad (3)$$

For 3C 293, $S_{CO}\,\Delta v = 51$ Jy km s^{-1} and $D_L = 180$ Mpc; thus $L'_{CO} = 3.8 \times 10^9$ K km s^{-1} pc^2. To calculate the mass of molecular gas in 3C 293, a reasonable assumption is made that the CO emission is optically thick and thermalized and that it originates in gravitationally bound molecular clouds. Thus, the ratio of the H_2 mass and the CO luminosity is given by $\alpha = M(H_2)/L'_{CO} \propto [n(H_2)]^{1/2}/T_b \ M_\odot$ (K km s^{-1} pc^2)$^{-1}$, where $n(H_2)$ and T_b are the density of H_2 and brightness temperature for the CO(1 → 0) transition (Scoville & Sanders 1987; Solomon, Downes, & Radford 1992). Multitransition CO surveys of molecular clouds in the Milky Way (e.g., Sanders et al. 1993) and in nearly

starburst galaxies (e.g., Güsten et al. 1993) have shown that hotter clouds tend to be denser such that the density and temperature dependencies tend to cancel each other. The variation in the value of α is approximately a factor of 2 for a wide range of kinetic temperatures, gas densities, and CO abundance (e.g., $\alpha = 2$–5 $M_\odot$ [K km s^{-1} pc^2]$^{-1}$; Radford, Solomon, & Downes 1991). We adopt a value of 4 $M_\odot$ (K km s^{-1} pc^2)$^{-1}$ for α, which is similar to the value determined for the bulk of the molecular gas in the disk of the Milky Way (Strong et al. 1988; Scoville & Sanders 1987).[4] Thus, the molecular gas mass of 3C 293 is 1.5×10^{10} $M_\odot$ (~5 times the molecular gas mass of the Milky Way); however, note that $M(H_2)$ could be as low as 7.3×10^9 $M_\odot$ (~2.5 times the Milky Way molecular gas mass). In addition, the concentration of molecular gas within the inner 3 kpc of 3C 293 is ~530 $M_\odot$ pc^{-2}. Such a molecular gas concentration is 4–400 times greater than that of nearby early-type spiral galaxies (e.g., Young & Scoville 1991) but on the low end of H_2 concentrations determined for a sample of $L_{IR} > 10^{11}$ $L_\odot$ merging galaxies studied by Scoville et al. (1991) and Bryant (1996).

4. DISCUSSION

As mentioned in § 1, several other radio galaxies have been detected in CO by single-dish telescopes. Millimeter interferometry of these radio galaxies is currently underway; for the present moment, the global properties of 3C 293 will be briefly compared with these radio galaxies before discussing 3C 293 in detail.

Table 1 summarizes the infrared and CO properties of 3C 293 relative to other CO-luminous radio galaxies. The galaxy 3C 293 is one of the most molecular gas rich of the radio galaxies detected to date but has a relatively low infrared luminosity and low L_{IR}/L'_{CO} ratio. The ratio L_{IR}/L'_{CO} is commonly referred to as the star formation "efficiency"; if the infrared luminosity is dominated by reprocessed light from young, massive stars, then the ratio indicates how efficiently molecular gas is converted into stars. In the case of 3C 293, a ratio of 8.9 indicates that the galaxy is producing stars at the rate of quiescent spiral galaxies (e.g., Sanders & Mirabel 1996). All of the more infrared luminous radio galaxies have very high L_{IR}/L'_{CO} ratios, but caution should be taken when interpreting their infrared luminosities; in the most luminous infrared galaxies, there is strong evidence that the infrared luminosity is heavily con-

---

[4] The equivalent $X_{CO} = n(H_2)/I_{CO} = 2.5 \times 10^{20}$ cm^{-2} (K km s^{-1})$^{-1}$.

TABLE 1

PROPERTIES OF CO-LUMINOUS RADIO GALAXIES

Parameter	3C 293	Other CO Luminous Radio Galaxies[a]
D_L (Mpc)	180	30–500
L_{IR} (8–1000 μm) ($\times 10^9$ $L_\odot$)	33	9–1700
z_{CO}	0.0446	0.0018–0.12
$S_{CO}\,\Delta v$ (Jy km s^{-1})	51 ± 11	30–200
Δv_{FWHM} (km s^{-1})	400	250–400
L'_{CO} ($\times 10^8$ K km s^{-1} pc^2)	3.7	2.5–120
$M(H_2)$ ($\times 10^9$ $M_\odot$)	15	1–50
L_{ir}/L'_{CO} ($L_\odot$/K km s^{-1} pc^2)	8.9	16–220

[a] Data of other CO-luminous radio galaxies have been compiled from the following sources: Phillips et al. 1987; Mirabel et al. 1989; Mazzarella et al. 1993; Evans et al. 1999a.
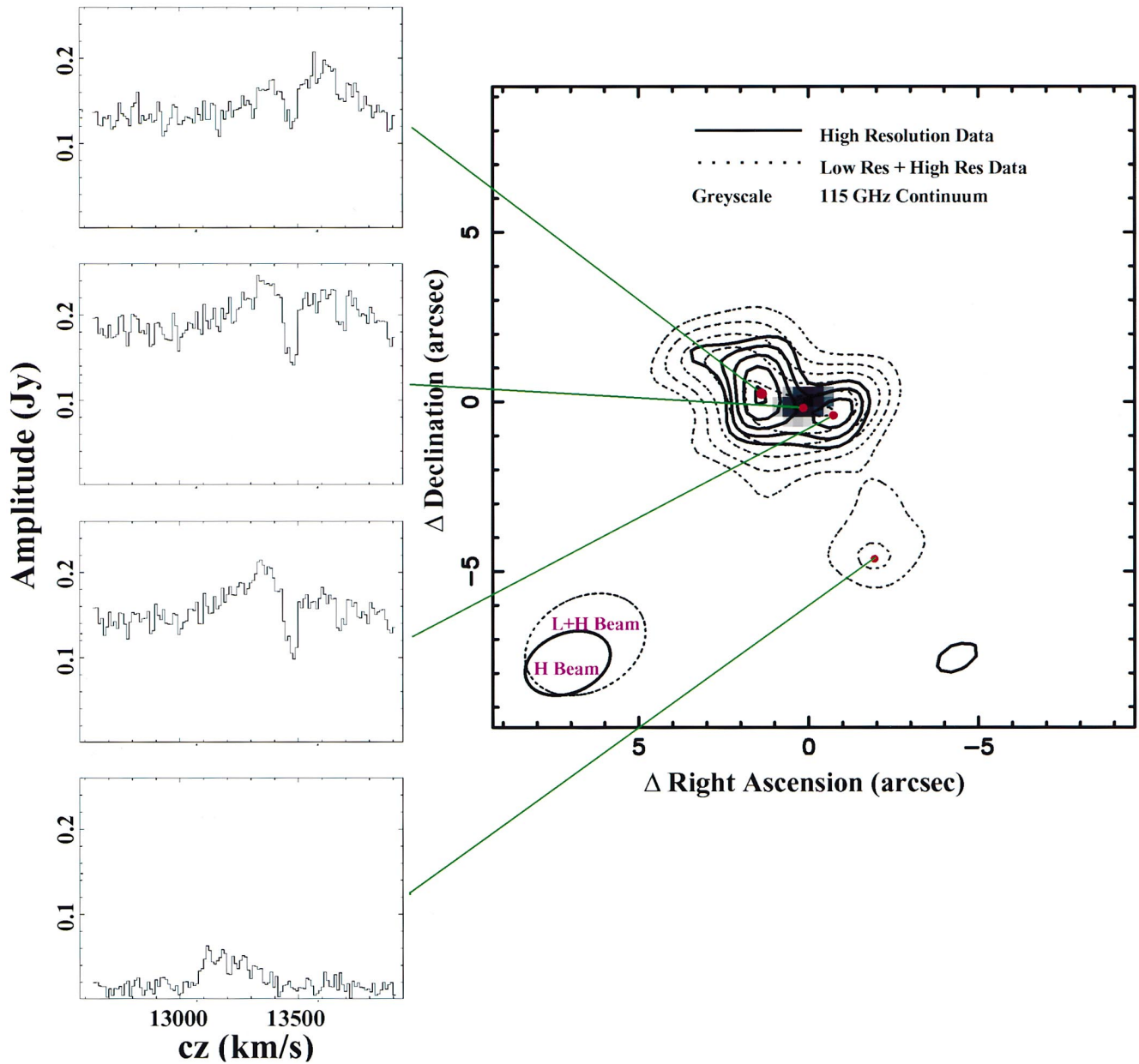
FIG. 3.—OVRO map of the CO($1 \rightarrow 0$) emission and 3 mm continuum emission in 3C 293. The continuum emission corresponds to a position of $13^h50^m03\overset{s}{.}20$, $+31°41'32\overset{''}{.}8$ (B1950.0). The 1 σ rms is 0.00436 and 0.00335 Jy beam^{-1} for the high and low+high resolution data, respectively. The high-resolution data are plotted as 60%, 70%, 80%, 90%, and 99% contours, where 60% corresponds to 3 σ rms and 100% corresponds to a peak flux of 0.0218 Jy beam^{-1}. The low+high resolution data are plotted as 50%, 60%, 70%, 80%, 90%, and 99% contours, where 50% corresponds to 3 σ rms and 100% corresponds to a peak flux of 0.0201 Jy beam^{-1}. Spectra extracted at several positions in the CO emission show clear evidence of rotation, as well as absorption associated with the central continuum source. The spectra have a 1 σ rms of 0.021 Jy per velocity channel, where the resolution of a single channel is ~ 10 km s^{-1}. A low-resolution CO map of 3C 293 can be found in Evans (1998).

taminated by reprocessed AGN light (e.g., Evans et al. 1998a). We will briefly return to this discussion in § 4.6.

4.1. *Optical Morphology*

Heckman et al. (1986) described 3C 293 as a primary galaxy connected to a southwestern companion galaxy by a bridge of emission that fans into a westward extending tidal tail beyond the companion. Although the images in Figure 1 do not have a wide enough field of view to show the tidal tail associated with the companion galaxy, Figure 1b clearly shows the low surface brightness emission that appears to be connecting the two galaxies. Indeed, the halo appears to completely envelope the primary galaxy.

The high surface brightness morphology of the primary galaxy is clearly that of a disk galaxy (Fig. 1a). The bulge component has redder colors than the disk component and contains a prominent, warped dust lane (see also van Breugel et al. 1984). The disk component also appears to be warped, but its apparent morphology may simply be an artifact of dust obscuration. It is not well understood what causes galaxy warps, but in the case of 3C 293, the warp may result from gravitational interactions with the companion galaxy, gas infall, and/or a misalignment between the disk and halo (e.g., Binney 1992).

4.2. *CO Emission*

The CO distribution of 3C 293 appears to be asymmetric

(Fig. 3) and may be subject to the same warping observed in the dust lanes and possibly the large-scale disk. As is clear from the four extracted spectra and CO morphology, the molecular gas is distributed in a disk rotating around the unresolved continuum source. Taking a disk radius of $3\rlap{.}''5$ (2.8 kpc) and a velocity width at half the maximum intensity of $\Delta v_{\mathrm{FWHM}} \sim 400$ km s^{-1}, the dynamical mass is

$$M_{\mathrm{dyn}} \approx \frac{r\Delta v_{\mathrm{FWHM}}^2}{\beta G \sin^2 i} = 1.0 \times 10^{11} \ [(\sin^2 i)^{-1} \ M_\odot] \ , \quad (4)$$

where G is the gravitational constant, i is the disk inclination, and β is approximately unity (e.g., Bryant & Scoville 1996). Thus the molecular gas mass is $\sim 10\%$ or less of the estimated dynamical mass. The remainder of the mass within this radius consists of stars and the central engine.

A molecular gas warp has been inferred in the radio galaxy Centaurus A by Quillen et al. (1992). From models of their single-dish telescope maps, Quillen et al. (1992) have speculated that the gas is in a triaxial potential. If the molecular gas in 3C 293 is also in such a potential, equation (4) may overestimate the true dynamical mass (i.e., if the gas is in elliptical orbits instead of circular). Thus the molecular gas in the inner 2.8 kpc may constitute more than 10% of the total estimated gas mass.

4.3. The 2.7 mm Continuum Emission

What is the source of the 2.7 mm continuum emission? The continuum emission, which has a flux density of 0.19 Jy, fits the extrapolated $f_\nu \propto \nu^{-\alpha}$ power-law relation of the higher frequency radio flux densities,[5] indicating that the 2.7 mm continuum emission is nonthermal.

As a double check, assume that the 2.7 mm emission is due to thermal emission from dust, as is the case for Arp 220. Arp 220, which is at a distance of 77 Mpc, has a 2.7 mm flux density of 0.035 Jy (Scoville, Yun, & Bryant 1997). Thus, the 2.7 mm luminosity of 3C 293 is 30 times higher than that of Arp 220. If the assumption is made, as for Arp 220, that the emission at $\lambda_0 > 200$ μm is emanating from optically thin ($\tau \sim 1$) dust radiating at a temperature of ~ 40 K, the dust mass is given by

$$M_{\mathrm{dust}} \approx \frac{S_{\mathrm{obs}} D_L^2}{(1 + z)\kappa_0 \, B(\nu_0, T)} \ , \quad (5)$$

where S_{obs} is the observed flux density, κ_0 is the rest-frequency mass absorption coefficient with a value of 0.085 g^{-1} cm^2 (i.e., 10 g^{-1} cm^2 at 250 μm scaled to 2.7 mm; Hildebrand 1983), and $B(\nu_0, T)$ is the rest-frequency value of the Planck function. The derived dust mass of 3C 293 is thus 2.0×10^{10} $M_\odot$. Further, if the dust in 3C 293 is radiating at a temperature of 15 K, the derived dust mass is a factor of 3 higher. Given that the standard gas-to-dust ratio is 100–200 and that the 2.7 mm continuum emission is not spatially extended like the CO emission, the 2.7 mm continuum emission is unlikely to be thermal emission emanating from dust associated with the molecular gas. Thus, the continuum emission most likely emanates from processes directly associated with a supermassive nuclear black hole or circumnuclear accretion disk.

4.4. The Nature of the CO Absorption

H I absorption features in several low-redshift radio galaxies have been extensively studied (e.g., Baan & Haschick

1981; Mirabel 1989; Conway & Blanco 1995). Such studies have attempted to determine the location and mass of H I within the host galaxies. In 3C 293, the depth of the CO absorption is shallower in the single-dish spectrum than in the OVRO spectrum, which indicates that beam dilution is masking the true absorption depth. Given this, the optical depth, τ_{CO}, of 3C 293 is $\tau \gtrsim \ln \ [I_{\mathrm{cont}}/(I_{\mathrm{cont}} - \Delta I_{\mathrm{abs}})] \gtrsim 0.69$, where I_{cont} is the continuum emission flux density and ΔI_{abs} is the CO absorption depth.

Although the velocity dispersions of individual absorbing clouds are probably typical of giant molecular clouds (i.e., $\lesssim 10$ km s^{-1}), the dispersion of the absorption feature ($\Delta v_{\mathrm{abs}} \sim 60$ km s^{-1}) may be due to the motion of the clouds around the nucleus of the galaxy. Assuming this is the case, the absorption occurs in clouds at a distance of $r_{\mathrm{cloud}} = M_{(<r)} G/\Delta v_{\mathrm{abs}}^2 \sim 120(M_{(<r)}/10^8 \ M_\odot)$ pc from the continuum source, where $M_{(<r)}$ is the stellar/gaseous/black hole mass interior to the absorbing clouds and G is the gravitational constant. This is comparable to the metric size of the dust torus surrounding the nucleus of the nearby FR II radio galaxy 3C 270 (NGC 4261), detected using the HST (Jaffe et al. 1996).

Is the velocity dispersion of the absorbing clouds really due to circumnuclear clouds in circular orbits? Similar stellar dispersion velocities have been observed in several galaxies believed to contain quiescent black holes (i.e., galaxies that may have once been radio galaxies or quasars); in the dwarf spheroidal M32, which is believed to possess a 2×10^6 $M_\odot$ black hole, the velocity dispersion is 60 km s^{-1} and increases to ~ 90 km s^{-1} within the central $1''$ (4 pc; e.g., Kormendy & Richstone 1995). The elliptical galaxy NGC 3377, believed to harbor a 2×10^8 $M_\odot$ black hole, has a velocity dispersion of 90 km s^{-1} that increases to ~ 158 km s^{-1} within the central $1''$ (48 pc; Kormendy et al. 1998). However, if the dynamical mass within the inner 2.8 kpc of 3C 293 is on the order of 1×10^{11} $M_\odot$, 3C 293 as a whole may have a mass comparable to a massive elliptical galaxy ($\gtrsim 3 \times 10^{11}$ $M_\odot$). Within 100 pc of the nucleus, the dispersion may actually be ~ 150–250 km s^{-1}, similar to those observed for NGC 3115 and NGC 4594 (The Sombrero Galaxy; e.g., Kormendy & Richstone 1995). The CO absorption may then be occurring in clouds in noncircular motion well outside of the circumnuclear region, as is believed to be the case for some of the clouds responsible for the molecular absorption observed in Centaurus A (Wiklind & Combes 1997).

4.5. Comparison between the CO Distribution of Radio Morphology

In Figure 4, the large-scale radio emission of 3C 293 (Leahy, Pooley, & Riley 1986) is superposed on the wide-field K'-band image. The large jets appear to be oriented nearly perpendicular to the major axis of the primary galaxy. Based on the major axis of the CO distribution (Fig. 3) and the large-scale structure, one might naively assume that the radio jets have simply escaped along the path of least resistance, the path perpendicular to the molecular gas and stellar distribution. Such a scenario would be consistent with the idea that the central engine is fed by a molecular torus/accretion disk and that the radio jets escape along the axis perpendicular to the accretion disk (e.g., Blandford 1984).

The structure in the inner few arcseconds, however, complicates matters: Figure 4a shows a high-resolution 5 GHz

---

[5] The radio densities were obtain from data compiled by the NASA Extragalactic Database (NED).
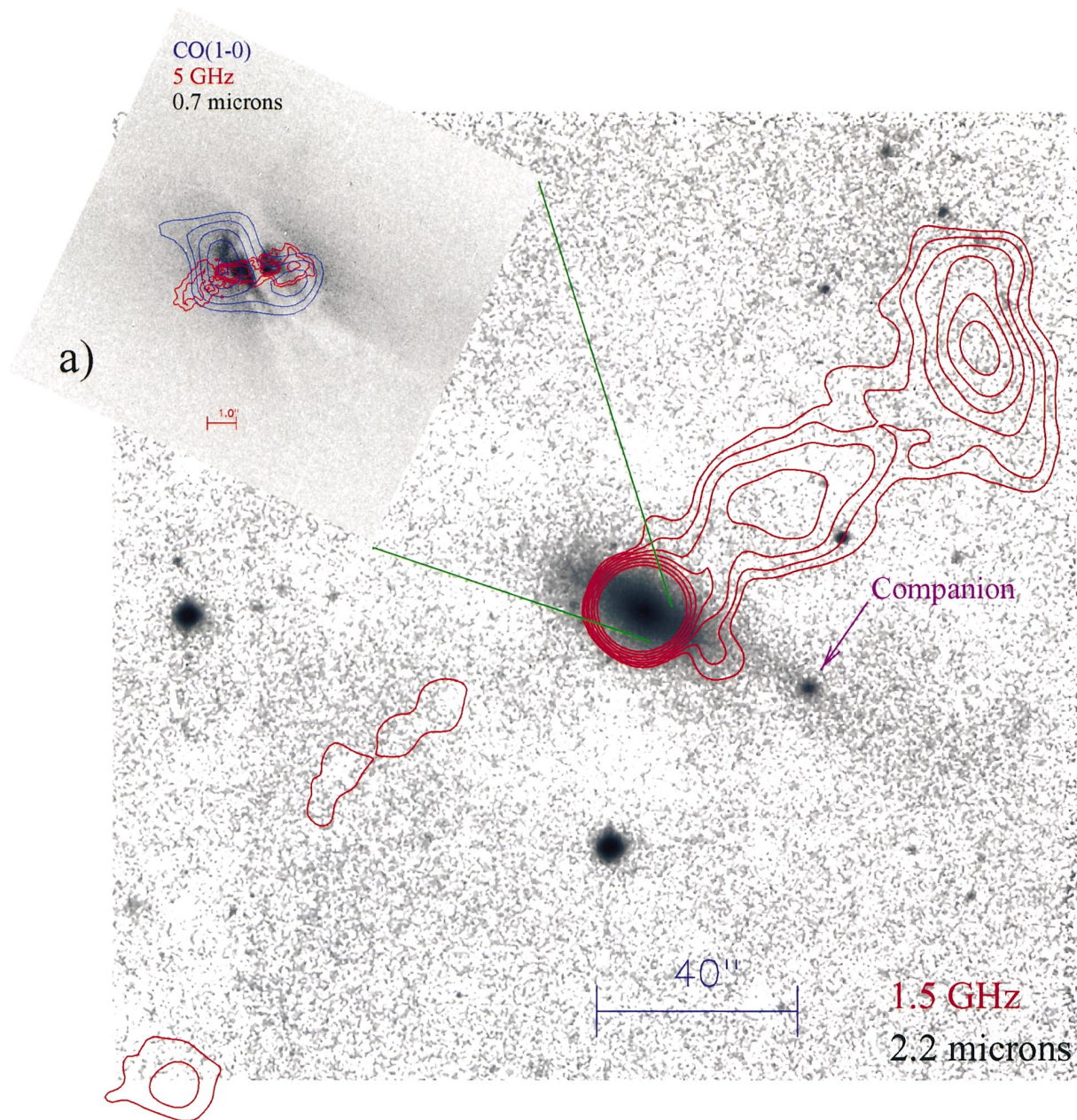
Fig. 4.—Radio (1.5 GHz) image of 3C 293 superposed on the logarithmic near-infrared (2.17 μm) image. The near-infrared image has been boxcar smoothed 4 × 4 pixels; the unsmoothed pixel scale is 0″.19 pixel^{-1}. (a) High-resolution 5 GHz MERLIN image and high-resolution CO(1 → 0) distribution (see Fig. 3) superposed on the 7000 Å HST image. The pixel scale of the 7000 Å image is 0″.046 pixel^{-1}. North is up, and east is to the left.

MERLIN map (Akujor et al. 1996) superposed on both the high-resolution CO map and an archival HST 7000 Å of 3C 293. The radio map has been registered with the CO map by assuming that the core of the 5 GHz emission is coincident with the 2.7 mm continuum emission (the coordinates of the 5 GHz core and the 2.7 mm continuum emission differ by less than 0″.3, which is much less than the resolution of the OVRO data). The registration of the MERLIN map with the HST image was done by first aligning the radio knots with features observed in a recently obtained near-infrared image of 3C 293 taken with the Near-Infrared Camera and Multiobject Spectrometer (NICMOS) aboard HST (Evans et al. 1999b). Such an alignment places the core of the 5 GHz emission on what appears to be the nucleus of the galaxy. Note that the nuclear dust lane observed in Figure 1

breaks up into multiple dust lanes in the HST image, which makes the nuclear region of 3C 293 resemble that of Centaurus A, which is dissected by a prominent warped dust lane (Sandage 1961).

The axis of the inner radio emission that extends 2″.5 (2.0 kpc) from the nucleus is rotated ~30° relative to the outer 1.5 GHz radio emission, which itself spans 200″ (160 kpc) from the tip of the bright northwest lobe to the tip of the fainter southeast lobe. Indeed, the twist of the eastern jet is apparent in the large-scale emission, which curves from the core toward the southern lobe. Such a jet morphology can be caused by (1) the redirection of the jets from a glancing impact with a molecular cloud or from a sudden change in the density gradient (e.g., van Breugel et al. 1984), (2) by a merger event or interaction, causing a warp in the

galaxy and thus shifting the radio axis (as in IRAS P09104+4109; Hines et al. 1999), or (3) by a precessing radio jet. The first scenario is supported by the fact that the eastern jet appears to twist northward after passing the 7000 Å off-nuclear knot, then southward after passing the centroid of the western CO component. At larger radii, the galactic density gradient would drive the large-scale radio emission to be perpendicular to the molecular and stellar distribution of the galaxy. However, it is difficult to reconcile this scenario with the relativistic velocity of the large-scale radio jets, as implied by the apparent Doppler boosting (dimming) of the approaching northwest (receding southeast) jets; an impact with molecular clouds would undoubtedly cause the inner jet to lose substantial amounts of kinetic energy. The second scenario is supported by the morphologies of the primary and companion galaxies (Fig. 1; Heckman et al. 1986). Given this, the inner radio jets may represent a more recent outburst triggered by a galaxy-galaxy interaction. Following Akujor et al. (1996), if it is assumed that the jet propagation speed is $0.1c$, the radio outburst resulting in the large-scale structure occurred 3×10^6 yr ago, and the companion outburst was produced only 3×10^4 yr ago. The third scenario is related somewhat to the second; the creation of a radio jet in a dynamically unrelaxed environment could result in the observed precession, and thus the high-resolution MERLIN map reflects the present pole axis of the supermassive black hole.

4.6. The Interaction/Merger Status of 3C 293

Much of the interpretation of the dynamic state of 3C 293 is dependent on whether or not the companion galaxy is the trigger for the strong interaction/merger. There is indeed strong morphological evidence that the companion is associated with 3C 293 (§ 4.1), but to our knowledge, there exists no published redshift of the companion. However, the companion appears to be a galaxy and not a foreground star; the measured FWHM of the companion in the 2.17 μm image is 2″1, as compared with 1″2 for stars in the field.

From the morphologies of 3C 293 and the companion, it might at first appear that the companion penetrated through the nuclear region of 3C 293 approximately (28 kpc/250 km s^{-1}) $\sim 1 \times 10^8$ yr ago, leaving a trail of optical/near-infrared debris (e.g., Figs. 1 and 4). Alternatively, the bridge of optical/near-infrared emission between 3C 293 and the companion may be a nonaxisymmetric tidal feature viewed nearly edge-on, created as the orbit of the companion decays via dynamical friction (see simulations by Hernquist & Mihos 1995). However, a determination of the relative masses of the two galaxies suggests that the companion is not massive enough to have caused the morphological disturbances observed in 3C 293 (Fig. 4a). The relative masses of the two galaxies can be estimated from the fact that the spectral energy distribution of supergiant stars peaks at ~ 1.6 μm, and thus the observed 2.17 μm luminosity is correlated with the mass of the galaxy. The ratio of companion mass to the mass of 3C 293 is therefore estimated to be ~ 0.03. Note that this ratio does not include light from the nucleus of 3C 293, which may emanate from the active galactic nucleus.

Given that interactions with the companion are an unlikely trigger for the present state of 3C 293, the linear feature extending from the host galaxy is most likely a tidal remnant from a merger event occurring more than 10^9 yr ago (see simulations by Barnes & Hernquist 1992, 1996).

Similar one-sided tidal features are observed in advanced mergers such as Mrk 273 (e.g., Mazzarella & Boroson 1993). A major difference between 3C 293 and advanced mergers such as Mrk 273, Arp 220, and the radio galaxy 3C 120 is that 3C 293 has a relatively low L_{IR}/L_{CO} ratio. This, however, may simply indicate that the star formation and/or AGN activity in 3C 293 that is typically responsible for boosting the infrared luminosity is waning.

The instabilities resulting from the merger have undoubtedly induced a loss of angular momentum in the molecular disk, causing a fraction of the gas to fall inward, ultimately serving as fuel for the nuclear activity. Eventually, the stellar distribution will dynamically relax into that of an elliptical or an early-type spiral galaxy, possibly making 3C 293 resemble more classical FR II radio galaxies such as Cygnus A.

5. SUMMARY

In this paper, the first detection of CO emission in an FR II type radio galaxy, the galaxy 3C 293, has been presented. The analysis of the CO data has benefited from data taken at a wide range of wavelengths. The following conclusions are drawn:

1. The optical morphology of 3C 293 shows a primary and what appears to be a companion galaxy enveloped by a low surface brightness halo, consistent with previous optical images of the galaxy. In addition, the primary galaxy has a warped dust lane and a possible warped disk, most likely resulting from an interaction/merger, gas infall, and/or misalignment between the disk and halo of the primary galaxy.

2. The CO emission line is relatively broad ($\Delta v_{FWHM} \sim 400$ km s^{-1}) and contains a $\Delta v_{abs} \sim 60$ km s^{-1} absorption feature at the same velocity as the H I absorption feature previously observed. Assuming the standard CO-to-H$_2$ mass conversion factor, the inferred molecular gas mass of 3C 293 is 1.5×10^{10} $M_\odot$.

3. The CO emission in 3C 293 is observed to be extended over a 7″ (5.7 kpc) diameter region, and the H$_2$ concentration within the inner 3 kpc is ~ 530 $M_\odot$ pc^{-2}. An unresolved, 2.7 mm continuum source is also detected, which is spatially coincident with the systemic absorption feature. The morphology and kinematics of the CO emission are consistent with a disk of molecular gas rotating around the continuum source.

4. The flux density of the 2.7 mm continuum source (0.19 Jy) is consistent with a power-law extrapolation of the radio wave flux densities. This, and the fact that the continuum emission is not coincident with the CO emission, indicates that the 2.7 mm continuum emission is nonthermal in nature and that it most likely emanates from a circumnuclear accretion disk around a supermassive black hole and not from dust associated with the molecular gas.

5. The radio jets of 3C 293 appear to twist by about 30° from the inner 10″ to the radio lobes. The cause of the twist is either due to the effects of a varying interstellar density gradient or precession, both of which are connected with a strong interaction or merger event in the recent history of 3C 293.

Based on the above conclusions, the observed properties of 3C 293 result from a strong interaction or merger event. The resultant instabilities have most likely induced gas in the inner molecular disk to lose angular momentum and fall

into the center of the gravitational potential well. Such a scenario provides a plausible explanation of how the central engines of radio galaxies are fueled.

REFERENCES

Akujor, C. E., Leahy, J. P., Garrington, S. T., Sanghera, H., Spencer, R. E., & Schilizzi, R. T. 1996, MNRAS, 278, 1
Baan, W. A., & Haschick, A. D. 1981, ApJ, 243, L143
Barnes, J., & Hernquist, L. 1992, ARA&A, 30, 705
———. 1996, ApJ, 471, 115
Binney, J. 1992, ARA&A, 30, 51
Blandford, R. D. 1984, in Eleventh Texas Symposium on Relativistic Astrophysics, ed. D. S. Evans (New York: New York Academy of Sciences), 422, 303
Bryant, P. M. 1996, Ph.D. thesis, California Institute of Technology
Bryant, P. M., & Scoville, N. Z. 1996, ApJ, 457, 678
Burbidge, E. M. 1967, ApJ, 149, L51
Conway, J. E., & Blanco, P. R. 1995, ApJ, 449, L131
Evans, A. S. 1998, in ASP Conf. Ser. 156, Highly Redshifted Radio Lines, ed. C. Carilli, S. J. E. Radford, K. Menten, & G. Langston (San Francisco: ASP), 74
Evans, A. S., Sanders, D. B., Cutri, R. M., Radford, S. J. E., Surace, J. A., Solomon, P. M., Downes, D., & Kramer, C. 1998a, ApJ, 506, 205
Evans, A. S., Sanders, D. B., Surace, J. A., & Mazzarella, J. M. 1999a, in preparation
Evans, A. S. et al. 1999b, in preparation
Fanaroff, B. L., & Riley, F. M. 1974, MNRAS, 167, 31P
Golombek, D., Miley, G. K., & Neugebauer, G. 1988, AJ, 95, 26
Güsten, R., Serabyn, E., Kasemann, C., Schinckel, A., Schneider, G., Schulz, A., & Young, K. 1993, ApJ, 402, 537
Heckman, T. M., et al. 1986, ApJ, 311, 526
Hernquist, L., & Mihos, J. C. 1995, ApJ, 448, 41
Hildebrand, R. H. 1983, QJRAS, 24, 267
Hines, D. C., Schmidt, G. D., Wills, B. J., Smith, P. S., & Sowinski, L. G. 1999, ApJ, in press
Hodapp, K., et al. 1996, New Astron., 1, 176
Jaffe, W., Ford, H., Ferrarese, L., van den Bosch, F., & O'Connell, R. W. 1996, ApJ, 460, 214
Kormendy, J., Bender, R., Evans, A. S., & Richstone, D. 1998, AJ, 115, 1823
Kormendy, J., & Richstone, D. 1995, ARA&A, 33, 581

Leahy, J. P., Pooley, G. G., & Riley, J. M. 1986, MNRAS, 222, 753
Mazzarella, J. M., & Boroson, T. A. 1993, ApJS, 85, 27
Mazzarella, J. M., Graham, J. R., Sanders, D. B., & Djorgovski, S. 1993, ApJ, 409, 170
Mirabel, I. F. 1989, ApJ, 340, L13
Mirabel, I. F., Sanders, D. B., & Kazès, I. 1989, ApJ, 340, L9
Phillips, T. G., et al. 1987, ApJ, 322, 73
Quillen, A. C., de Zeeuw, P. T., Phinney, E. S., & Phillips, T. G. 1992, ApJ, 391, 121
Radford, S. J. E., Solomon, P. M., & Downes, D. 1991, ApJ, 368, L15
Sandage, A. 1961, The Hubble Atlas of Galaxies (Washington, DC: Carnegie Institute of Washington)
———. 1966, ApJ, 145, 1
Sanders, D. B., & Mirabel, I. F. 1996, ARA&A, 34, 749
Sanders, D. B., Scoville, N. Z., & Soifer, B. T. 1991, ApJ, 370, 158
Sanders, D. B., Scoville, N. Z., Tilanus, R. P. J., Wang, Z., & Zhou, S. 1993, in Back to the Galaxy, ed. S. Holt & F. Verter (New York: AIP), 311
Scoville, N. Z., Carlstrom, J. C., Chandler, C. J., Phillips, J. A., Scott, S. L., Tilanus, R. P., & Wang, Z. 1992, PASP, 105, 1482
Scoville, N. Z., & Sanders, D. B. 1987, in Interstellar Processes, ed. D. Hollenbach & H. Thronson (Dordrecht: Reidel), 21
Scoville, N. Z., Sargent, A. I., Sanders, D. B., & Soifer, B. T. 1991, ApJ, 366, L5
Scoville, N. Z., Yun, M. S., & Bryant, P. M. 1997, ApJ, 484, 702
Shepherd, M. C., Pearson, T. J., & Taylor, G. B. 1995, BAAS, 27, 903
Smith, E. P., & Heckman, T. M. 1989a, ApJS, 69, 365
———. 1989b, ApJ, 341, 658
Solomon, P. M., Downes, D., & Radford, S. J. E. 1992, ApJ, 398, L29
Strong, A. W., et al. 1988, A&A, 207, 1
van Breugel, W., Heckman, T., Butcher, H., & Miley, G. 1984, ApJ, 277, 82
Wainscoat, R. J. 1996, University of Hawaii Telescopes at Telescopes at Mauna Kea Observatory—User Manual, Univ. Hawaii
Wiklind, T., & Combes, D. 1997, A&A, 324, 51
Young, J. S., & Scoville, N. Z. 1991, ARA&A, 29, 581